

General analysis of instabilities in erbium-doped fiber lasers

François Sanchez* and Guy Stephan†

Ecole Nationale Supérieure de Sciences Appliquées et de Technologie, Laboratoire d'Optronique, 6, rue de Kérampont, Boîte Postale 447, 22305 Lannion, France

(Received 14 July 1995)

A detailed analysis of a general model of erbium-doped fiber laser dynamics is investigated. Depending upon the parameters the same model describes single-mode cw or self-pulsing lasers, dual-wavelength or bipolarized two-mode lasers. A summary of previous works concerning self-pulsing behavior and antiphase phenomena is presented. The basic physics responsible for the instabilities is the existence of ion clusters in heavily doped fibers. A thorough investigation of the bimode laser equations is performed. Approximate solutions for the steady states and for the second threshold are obtained. The influence of ion-pair concentration (x) on dynamical behavior is studied. In particular, it is demonstrated that optical bistability occurs between $2T$ - and $3T$ -periodic orbits versus the pumping rate in the case of intermediate pair concentrations (where T is the fundamental period of the system). The route to chaos is found to be x dependent and of codimension 2.

PACS number(s): 42.65.Sf, 42.60.Mi, 42.55.-f, 42.50.Lc

I. INTRODUCTION

The field of rare-earth-doped fiber lasers is actually an expanding area of investigation [1–4]. This growing interest is essentially due to the large number of possibilities given by this new kind of coherent sources. Indeed, in addition to their applications to telecommunications or to visible solid-state laser engineering (ZBLAN-doped fibers are very attractive for the development of up-conversion lasers), fiber lasers are excellent candidates for dynamical studies, in particular in the frame of multimode lasers [5–8]. In spite of their very large degree of freedom (some thousands of longitudinal modes can typically coexist), fiber lasers can be theoretically described by very low-dimensional systems [1,2,8,9]. This is allowed because a clustering effect occurs between hundreds of modes [2,9]. The physics of this collective behavior is actually not well understood.

Among the different dopants which can be incorporated in silicate fibers, neodymium and erbium have been the subject of particular attention. Nd-doped fiber lasers have revealed interesting polarization properties under pump modulation conditions [2,8,10]. Spontaneous trains of pulses can also be obtained (for a cw operating fiber laser) under specific experimental conditions (tilt of the output coupling mirror); this dynamical behavior is not yet physically understood [10].

Er-doped fiber lasers (EDFLs) are, in some sense, more interesting due to the large variety of dynamics which can be obtained spontaneously. Self-pulsing operation was reported in EDFLs; this behavior was found to be independent of the pumping wavelength, the fiber length, and the photon lifetime in the cavity [11]. The self-pulsing suggested the existence of a saturable absorber,

distributed within the doped fiber, which has been identified as ion pairs (or ion clusters) [12]. The physical effect leading to the saturable absorption is a fast nonradiative energy transfer between two excited neighboring ions [12]. A simple modeling of EDFL dynamics has been proposed and investigated in [1] assuming the amplifying medium as a mixture of isolated ions and ion pairs. More recently, similar results have been reported [13]; nevertheless, the saturable absorber is not clearly identified. A more complex dynamics (antiphase effects and chaotic behavior) has been reported [3,14] for dual-wavelength operation of EDFLs. An extension of the single-mode model [1] to a two-mode laser was proposed and investigated [9]. The numerical analysis was, however, restricted to the intermediate ion-pair concentration case.

The aim of this paper is to present a general theoretical analysis of EDFL instabilities under autonomous conditions (without pump or other external modulation). A synthesis of previous works is included in the paper together with a great amount of new results. This article is organized as follows. Section II is devoted to the single-mode model. A summary of the results developed in [1] is given first. Then an approximate solution for the steady-state intensity is derived using a method which takes advantage of the saturation of the gain. The two-mode model is presented in Sec. III. This model is general enough to be used for bipolarized or dual-wavelength EDFL operations. In addition, it can be reduced to the single-mode model under some conditions. A thorough investigation of the stationary states (off state, single-mode states, and bimode state) and their stability is performed in Sec. IV. In particular, we give approximate solutions for the intensities leading to a closed form approximate expression for the second threshold. The approximate solutions allow a simple experimental evaluation of the anisotropic pumping parameter. In Sec. V we investigate numerically the dynamical behavior obtained for different ion-pair concentrations (x). This analysis was performed in [9] in the particular case where

*Electronic address: sanchez@enssat.fr

†Electronic address: stephan@enssat.fr

$x = 10\%$. We are particularly interested in both routes to chaos and bistability between periodic orbits. Concluding remarks and perspectives are given in Sec. VI.

II. THE SINGLE-MODE MODEL

In this section we briefly recall the results presented in [1,11,12] and give our results concerning the approximate solution for the steady-state intensity in EDFs. In the simplest experimental configuration (two-mirror cavities with fiber ends directly butted on the mirrors) EDFs can operate spontaneously in a self-pulsing or cw regime around $\lambda = 1.55 \mu\text{m}$ (corresponding to the ${}^4I_{13/2} \rightarrow {}^4I_{15/2}$ transition). This behavior has been attributed to the existence of ion clusters (ion pairs) which act as saturable absorbers [12]. The basic effect responsible for this saturable absorption is the quenching effect which occurs between two neighboring ions. This is illustrated in Fig. 1: when two neighboring ions are in the ${}^4I_{13/2}$ excited state, there occurs a fast ($\tau \approx \text{some } \mu\text{s}$ [1]) energy transfer resulting in one ground-state ion and one up-converted ion which quickly spontaneously relaxes towards the ${}^4I_{13/2}$ state. The consequence of this energy transfer is the loss of one excited ion and therefore of one potential stimulated photon. This explains why long and weakly doped fibers are preferred to short and heavily doped fibers in Er^{3+} -doped fiber amplifiers [15,16].

As reported in [12], for low ion-pair concentration ($x < 5\%$) a cw regime occurs, while a self-pulsing behavior is observed for high x ($x > 10\%$), for any pumping rate in both cases. For intermediate x values ($x = 7.5\%$), the laser is self-pulsing in the range $r = 1-5$ (r is the pumping ratio defined as $r = \Lambda/\Lambda_{\text{th}}$, where Λ_{th} is the threshold pump power). Basically, as the Er^{3+} concentration increases, x increases [12,17-19]. It has been theoretically demonstrated [1] that the dynamics of EDFL depends on the ion-pair concentration and the pumping ratio. More recently, the spontaneous emission factor has been found to influence the stability of the laser [20]: spontaneous emission stabilizes the system near threshold.

In [1] the amplifying medium (the doped fiber) is considered to be a mixture of isolated ions and ion pairs. Isolated ions are described as two-level systems and ion pairs as three-level systems (Fig. 2). The dynamics of the laser is modeled with the following nonlinear differential normalized system [1]:

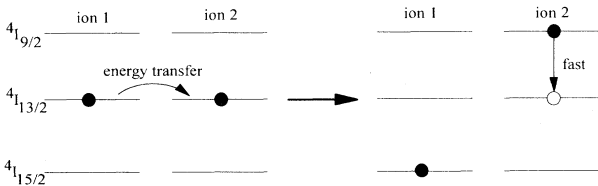


FIG. 1. Quenching effect in ion pairs.

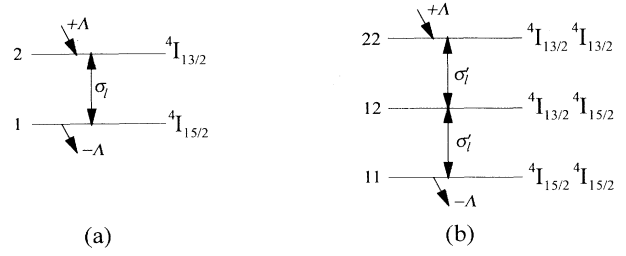


FIG. 2. Energy levels of (a) isolated ion and (b) ions pairs.

$$\begin{aligned} \frac{\partial d}{\partial t} &= \Lambda - a_2(1+d) - 2Id, \\ \frac{\partial d_+}{\partial t} &= a_2(1-d_+) - a_{22}(d_+ + d_-)/2 + yI(2-3d_+), \\ \frac{\partial d_-}{\partial t} &= \Lambda - a_2(1-d_+) - a_{22}(d_+ + d_-)/2 - yId_-, \\ \frac{\partial I}{\partial t} &= -I + A(1-2x)Id + AxyId_-, \end{aligned} \quad (1)$$

where $d = n_2 - n_1$ is the population inversion for isolated ions, $d_{\pm} = n_{22} \pm n_{11}$ with n_{22} and n_{11} are the populations of levels 22 and 11 (see Fig. 2), I is the laser intensity, Λ is the pumping parameter, $y = \sigma'_1/\sigma_l$ where the σ s are the absorption cross sections (see Fig. 2), $A = \sigma_l N_0 \tau_l$, $a_2 = \tau_1/\tau_2$, $a_{22} = \tau_1/\tau_{22}$, where N_0 is the erbium concentration, τ_l is the photon lifetime in the cavity, and τ_2 and τ_{22} are, respectively, the lifetimes of level 2 and 22. The time is normalized versus the photon lifetime. For our purpose, noise due to spontaneous emission is neglected here.

The steady state is easily obtained for the population terms [1]

$$\begin{aligned} \bar{d} &= \frac{\Lambda - a_2}{a_2 + 2\bar{I}}, \\ \bar{d}_- &= \frac{-2a_2a_{22} + \Lambda(a_{22} + 2a_2) - 2y(a_2 + a_{22} + 3\Lambda)\bar{I}}{2(a_2a_{22} + y(a_2 + 2a_{22})\bar{I} + 3y^2\bar{I}^2)}, \end{aligned} \quad (2)$$

$$\bar{d}_+ = \frac{2a_2a_{22} - a_{22}\Lambda + 2y(a_2 + a_{22})\bar{I} + 4y^2\bar{I}^2}{2(a_2a_{22} + y(a_2 + 2a_{22})\bar{I} + 3y^2\bar{I}^2)},$$

where the bars stand for the steady-state values.

In [1], the steady-state intensity is one of the solutions of a third order polynomial equation and has been calculated numerically. We use here a method which allows us to obtain an approximate closed form expression for the intensity. The starting point is the fact that the gain saturates to its value at laser threshold (whatever the pump above threshold, one always has gain plus losses equal to 0). In these conditions, one can write the following con-

servation relation:

$$(1-2x)\frac{\partial \bar{d}}{\partial \Lambda} + xy\frac{\partial \bar{d}_-}{\partial \Lambda} = 0. \tag{3}$$

In fact, the last relation is a direct consequence of (1) at steady state. Relation (3) gives an equation for $\partial \bar{I} / \partial \Lambda$ which can be estimated at laser threshold leading to the slope of the laser characteristic at threshold:

$$\left. \frac{\partial \bar{I}}{\partial \Lambda} \right|_{\Lambda_{th}} = \frac{A [2a_{22}(1-2x) + xy(a_{22} + 2a_2)]^2}{8a_{22}^2(1-2x) + 2A(a_{22} - 2a_2)(1-2x)xy(2a_{22} - ya_2) + 2(2a_2^2 + 2a_{22}^2 - a_2a_{22})xy^2 + 2A(2a_2^2 - 3a_2a_{22} + a_{22}^2)x^2y^3}. \tag{A4}$$

An approximate solution for the steady-state intensity can thus be written assuming a linear characteristic versus the pumping parameter:

$$\bar{I}(\Lambda) = \left. \frac{\partial \bar{I}}{\partial \Lambda} \right|_{\Lambda_{th}} (\Lambda - \Lambda_{th}). \tag{5}$$

In fact, it can be easily demonstrated that the evolution of the intensity versus the pumping rate is slightly non-linear in single-mode EDFL, the difference with linearity remaining very weak in the range $r = 1-3$. The lasing threshold is [1]

$$\Lambda_{th} = \frac{2a_2a_{22}}{A} \frac{1 + (1-2x)A + xyA}{2a_{22}(1-2x) + xy(2a_2 + a_{22})}. \tag{6}$$

The linear stability analysis of (1) around its steady state leads to the following characteristic equation for the eigenvalues [1]:

$$(\lambda - \lambda_1)(\lambda - \lambda_2)(\lambda - \lambda_3)(\lambda - \lambda_3^*) = 0, \tag{7}$$

where λ_1, λ_2 are real negative numbers for any pumping ratio ($r = \Lambda / \Lambda_{th}$) and $\lambda_3 = \alpha + i\omega$. The damping coefficient α is negative for any r at low pair concentra-

tions (stability of the steady state) and positive in some range of pumping rates for higher x (unstable steady states: in this case stable self-pulsing solutions are obtained). ω is the eigenfrequency of the system and varies as $\sqrt{\Lambda - \Lambda_{th}}$. It is convenient to represent the dynamical behavior in a stability diagram which gives for any x the particular r values for which α vanishes (Hopf bifurcation [21]). The theoretical results are given in Fig. 3; open circles correspond to experimental data from [12]. This representation clearly shows the cw and self-pulsing domains. Figure 4(a) shows an example of the self-

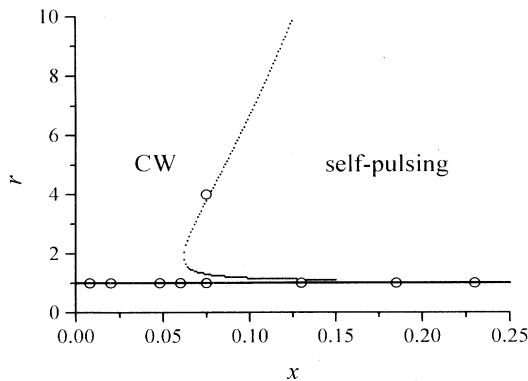


FIG. 3. Stability diagram: theory (with $\tau_l = 10$ ns) and experiment.

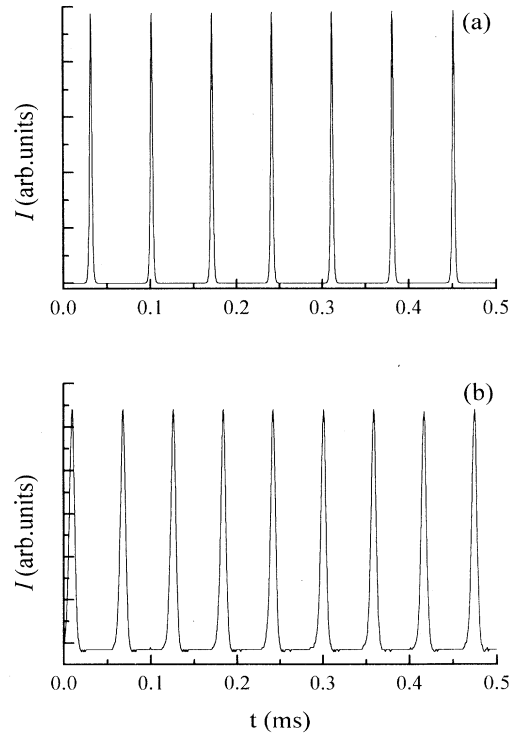


FIG. 4. (a) Example of self-pulsing operation obtained by numerical integration of system (1) for $x = 10\%$, $r = 1.5$. (b) Experimental self-pulsing obtained with an erbium-doped fiber having $x = 18\%$ at two times threshold (from [12]).

pulsing operation obtained by numerical integration of system (1) in the case $x = 10\%$ and for a pumping ratio $r = 1.5$. Note that the pulse period is about $80 \mu\text{s}$, which is in very good agreement with experimental data from [11]. Figure 4(b) shows the experimental periodic self-pulsing operation in the case $x = 18\%$ and $r = 2.0$. The period is $60 \mu\text{s}$ in this particular case.

III. THE TWO-MODE MODEL

Antiphase dynamics and chaos have been reported when erbium-doped fiber lasers operate simultaneously on two modes or two clusters of modes around $\lambda = 1.55$ and $1.536 \mu\text{m}$ [3,14] (similar results have also been reported for resolved polarization eigenstates in EDFLs [13]). The antiphase states correspond to the two mode intensities related to the two wavelengths. In [14], experimental results obtained with a fiber having a pair concentration $x = 18.5\%$ was reported. The dynamical behavior was typically chaotic (spontaneous train of irregular pulses) with particular periodic windows ($2T$ and $3T$) depending on the experimental conditions. Antiphase dynamics occurred between the two modes. In [3], the same experiment was performed with a doped fiber with intermediate pair concentration ($x = 7.5\%$). In this case, starting from a stable cw state achieved at high pumping level, it is possible to follow the evolution for decreasing r . The scenario is typically $\text{cw} \rightarrow T$ periodic $\rightarrow 2T$ periodic $\rightarrow 3T$ periodic \rightarrow chaos $\rightarrow T$ periodic. A simple modeling of this behavior is achieved with a classical two-mode laser model including population dynamics of ion pairs. This theory is developed in Refs. [3,9] and investigated numerically for intermediate pair concentrations and only above the second threshold. In the following, we present an in-depth study of the bimode model. In particular, the linear stability analysis is presented for all the stationary states: off state, single-mode states, and two-mode state. Moreover, the derivation of approximate solutions for the intensities leads to a closed form expression for the second threshold, allowing a simple evaluation of the anisotropic pumping parameter.

The dynamics of two-mode EDFLs is monitored by the following equations [3]:

$$\frac{\partial d_1}{\partial t} = \Lambda - a_2(1 + d_1) - 2d_1(I_1 + \beta I_2), \quad (8a)$$

$$\frac{\partial d_2}{\partial t} = \gamma \Lambda - a_2(1 + d_2) - 2d_2(\beta I_1 + I_2), \quad (8b)$$

$$\frac{\partial d_+}{\partial t} = a_2(1 - d_+) - a_{22}(d_+ + d_-)/2 + y(I_1 + I_2)(2 - 3d_+), \quad (8c)$$

$$\frac{\partial d_-}{\partial t} = \Lambda - a_2(1 - d_+) - a_{22}(d_+ + d_-)/2 - y(I_1 + I_2)d_-, \quad (8d)$$

$$\frac{\partial I_1}{\partial t} = [-1 + A(1 - 2x)(d_1 + \beta d_2) + Ad_-xy]I_1, \quad (8e)$$

$$\frac{\partial I_2}{\partial t} = [-1 + A(1 - 2x)(d_2 + \beta d_1) + Ad_-xy]I_2, \quad (8f)$$

where γ is the anisotropic pumping parameter and β the cross-saturation parameter. Equations (8a), (8b), (8c), and (8f) correspond to a classical two-mode laser and Eqs. (8c) and (8d) to the dynamics of ion pairs. In the following we consider (without loss of generality) $\gamma < 1$. In such conditions the first lasing mode is always I_1 .

This model includes the single-mode model with the following adaptation of the parameters: $\gamma = 1, \beta = 0, d = (d_1 + d_2)/2, I = I_1 + I_2$.

IV. STATIONARY STATES AND THEIR STABILITY

This section is devoted to the study of the stability of the different stationary states. Approximate solutions for the intensities and the second threshold are derived and lastly compared to exact solutions.

A. Off state

The off state is characterized by $I_1 = 0, I_2 = 0$ and is stable for $0 \leq \Lambda \leq \Lambda_{\text{th}}$. The steady state is easily obtained from system (8):

$$\begin{aligned} \bar{d}_1 &= \frac{\Lambda}{a_2} - 1, \quad \bar{d}_2 = \gamma \frac{\Lambda}{a_2} - 1, \\ \bar{d}_+ &= 1 - \frac{\Lambda}{2a_2}, \quad \bar{d}_- = \Lambda \left[\frac{1}{a_{22}} + \frac{1}{2a_2} \right] - 1. \end{aligned} \quad (9)$$

The linear stability analysis leads to the following eigenvalues:

$${}^0\lambda_1 = -a_2 \quad (\text{threefold degenerate}),$$

$${}^0\lambda_2 = -a_{22},$$

$${}^0\lambda_3 = -1 + A(1 - 2x)(\bar{d}_1 + \beta \bar{d}_2) + Axy\bar{d}_-$$

associated to I_1 ,

$${}^0\lambda_4 = -1 + A(1 - 2x)(\bar{d}_2 + \beta \bar{d}_1) + Axy\bar{d}_-$$

associated to I_2 . All are real and negatives below the first laser threshold Λ_{th} . For $\Lambda = \Lambda_{\text{th}}$, ${}^0\lambda_3$ vanishes and becomes positive up to the first threshold (instability of the off state above the first lasing threshold). This allows the derivation of Λ_{th} :

$$\Lambda_{\text{th}} = \frac{2a_2a_{22}}{A} \frac{1 + A(1 - 2x)(1 + \beta) + Axy}{2a_{22}(1 + \beta\gamma)(1 - 2x) + xy(2a_2 + a_{22})}. \quad (10)$$

B. Single-mode states

The only single-mode state of interest is characterized by $I_1 \neq 0, I_2 = 0$ and is stable for $\Lambda_{\text{th}} \leq \Lambda \leq \Lambda_{\text{th}}^2$. With the usual terminology, I_1 is the strong mode. The other single-mode state is unstable due to the choice of $\gamma < 1$ and its threshold is greater than the other. The steady state is easily derived for the populations

$$\begin{aligned}\bar{d}_1 &= \frac{\Lambda - a_2}{a_2 + 2\bar{I}_1}, \\ \bar{d}_2 &= \frac{\gamma\Lambda - a_2}{a_2 + 2\bar{I}_1}, \\ \bar{d}_- &= \frac{-2a_2a_{22} + \Lambda(a_{22} + 2a_2) - 2y(a_2 + a_{22} + 3\Lambda)\bar{I}_1}{2(a_2a_{22} + y(a_2 + 2a_{22})\bar{I}_1 + 3y^2\bar{I}_1^2)}, \\ \bar{d}_+ &= \frac{2a_2a_{22} - a_{22}\Lambda + 2y(a_2 + a_{22})\bar{I}_1 + 4y^2\bar{I}_1^2}{2(a_2a_{22} + y(a_2 + 2a_{22})\bar{I}_1 + 3y^2\bar{I}_1^2)}.\end{aligned}\quad (11)$$

An approximate solution for the strong mode can be written

$$\bar{I}_1(\Lambda) = \frac{\Lambda - {}^1\Lambda_{\text{th}}}{2\Lambda_{\text{th}} - {}^1\Lambda_{\text{th}}} \bar{I}({}^2\Lambda_{\text{th}}). \quad (12)$$

Relation (12) is simply the equation of the straight line connecting the point $({}^1\Lambda_{\text{th}}; \bar{I}_1=0)$ to $({}^2\Lambda_{\text{th}}; \bar{I}_1({}^2\Lambda_{\text{th}}))$, in order to obtain a continuous characteristic versus pumping rate using the approximate solutions above the second threshold.

The linear stability analysis leads to the characteristic equation

$$(\lambda - {}^s\lambda_5)P(\lambda) = 0, \quad (13)$$

where $P(\lambda)$ is a polynomial of fifth degree and

$${}^s\lambda_5 = -1 + A(1-2x)(\bar{d}_2 + \beta\bar{d}_1) + Axy\bar{d}_-.$$

The second threshold is reached when ${}^s\lambda_5$ vanishes (instability of the single-mode solution). $P(\lambda)$ can be written in the form

$$\begin{aligned}P(\lambda) &= (\lambda - {}^s\lambda_1)(\lambda - {}^s\lambda_2)(\lambda - {}^s\lambda_3) \\ &\quad \times (\lambda - {}^s\lambda_4)(\lambda - {}^s\lambda_4^*),\end{aligned}\quad (14)$$

where ${}^s\lambda_1, {}^s\lambda_2, {}^s\lambda_3$ are real negative numbers for any pumping ratio and ${}^s\lambda_4 = \alpha_s + i\omega_s$. Depending on the ion-pair concentration, α_s can be positive, leading to a stable self-pulsing operation. ω_s is the eigenfrequency of the system and is responsible for the relaxation oscillations. As in the case of the single-mode model, the frequency evolves according to $\sqrt{\Lambda - {}^1\Lambda_{\text{th}}}$.

C. Bimode state

The bimode state is characterized by $I_1 \neq 0, I_2 \neq 0$ and is stable for $\Lambda \geq {}^2\Lambda_{\text{th}}$. In order to derive the steady state, let us introduce the more convenient variables defined by [9]

$$\begin{aligned}D &= (d_1 + d_2), \\ d &= (d_1 - d_2), \\ I &= (I_1 + I_2), \\ i &= (I_1 - I_2).\end{aligned}\quad (15)$$

With these new variables, system (7) becomes

$$\begin{aligned}\frac{\partial D}{\partial t} &= -2a_2 - a_2D + \Lambda(1+\gamma) - d(1-\beta)i - D(1+\beta)I, \\ \frac{\partial d}{\partial t} &= -a_2d + \Lambda(1-\gamma) - D(1-\beta)i - d(1+\beta)I, \\ \frac{\partial d_+}{\partial t} &= a_2(1-d_+) - a_{22}(d_- + d_+)/2 + (2-3d_+)Iy, \\ \frac{\partial d_-}{\partial t} &= \Lambda - a_2(1-d_+) - a_{22}(d_- + d_+)/2 - d_-Iy, \\ \frac{\partial I}{\partial t} &= \frac{Ad}{2}(1-\beta)(1-2x)i \\ &\quad + \left[-1 + \frac{AD}{2}(1+\beta)(1-2x) + Ad_-xy \right] I, \\ \frac{\partial i}{\partial t} &= \frac{Ad}{2}(1-\beta)(1-2x)I \\ &\quad + \left[-1 + \frac{AD}{2}(1+\beta)(1-2x) + Ad_-xy \right] i.\end{aligned}\quad (16)$$

The steady-state values of the populations and i can be expressed as functions of I [9]:

$$\begin{aligned}\bar{d} &= 0, \\ \bar{D} &= \frac{-2a_2 + \Lambda(1+\gamma)}{a_2 + \bar{I} + \beta\bar{I}}, \\ \bar{d}_- &= \frac{-2a_2a_{22} + 2a_2\Lambda + a_{22}\Lambda - 2a_2\bar{I}y - 2a_{22}\bar{I}y + 6\Lambda\bar{I}y}{2(a_2a_{22} + a_2\bar{I}y + 2a_{22}\bar{I}y + 3\bar{I}^2y^2)}, \\ \bar{d}_+ &= \frac{2a_2a_{22} - a_{22}\Lambda + 2a_2\bar{I}y + 2a_{22}\bar{I}y + 4\bar{I}^2y^2}{2(a_2a_{22} + a_2\bar{I}y + 2a_{22}\bar{I}y + 3\bar{I}^2y^2)}, \\ \bar{i} &= \frac{\Lambda(1-\gamma)(a_2 + \bar{I} + \beta\bar{I})}{(-1+\beta)(2a_2 - \Lambda - \Lambda\gamma)}.\end{aligned}\quad (17)$$

Using the same procedure as that used for the single-mode model, we can write the following conservation relation in order to derive an approximate solution for the total intensity I :

$$(1+\beta)(1-2x)\frac{\partial \bar{D}}{\partial \Lambda} + 2xy\frac{\partial \bar{d}_-}{\partial \Lambda} = 0. \quad (18)$$

This equation leads to the slope of the total intensity estimated at its extrapolated threshold:

$$\frac{\partial \bar{I}}{\partial \Lambda} \Big|_{\Lambda'_{th}} = \frac{a_2 a_{22} [a_{22} \tilde{\beta} \tilde{\gamma} (1-2x) + xy(a_{22} + 2a_2)]}{\Lambda'_{th} [a_{22}^2 \tilde{\beta}^2 (1-2x) + xy^2 (2a_2^2 - a_2 a_{22} + 2a_{22}^2)] - 2a_2 a_{22}^2 [\tilde{\beta}^2 (1-2x) + xy^2]} , \quad (19)$$

with the notations $\tilde{\beta} = \beta + 1$ and $\tilde{\gamma} = \gamma + 1$. Λ'_{th} is the threshold for I (very close to the first laser threshold [9]) [3]:

$$\Lambda'_{th} = \frac{2a_2 a_{22}}{A} \frac{1 + A(1-2x)\tilde{\beta} + Axy}{a_{22}(1-2x)\tilde{\beta}\tilde{\gamma} + xy(2a_2 + a_{22})} . \quad (20)$$

An approximate solution for the total intensity is therefore obtained:

$$\bar{I}(\Lambda) = \frac{\partial \bar{I}}{\partial \Lambda} \Big|_{\Lambda'_{th}} (\Lambda - \Lambda'_{th}) . \quad (21)$$

The difference intensity is related to the total intensity through the relation

$$\bar{i} = - \frac{\Lambda(1-\gamma)}{(1-\beta)} \frac{a_2 + (1+\beta)\bar{I}}{2a_2 - \Lambda(1+\gamma)} . \quad (22)$$

The approximate solution at first order in Λ is

$$\bar{i} = \frac{\Lambda(2-\tilde{\gamma})}{\tilde{\gamma}(2-\tilde{\beta})} \frac{a_2 a_{22} \tilde{\beta} [a_{22} \tilde{\beta} \tilde{\gamma} (1-2x) + xy(2a_2 + a_{22})]}{\Lambda'_{th} [xy^2 (2a_2^2 - a_2 a_{22} + 2a_{22}^2) + a_{22} \tilde{\beta}^2 \tilde{\gamma} (2a_2 + a_{22})] - 2a_2 a_{22}^2 [xy^2 + \tilde{\beta}^2 (1-2x)]} . \quad (23)$$

The threshold for the second mode ${}^2\Lambda_{th}$ is achieved when $\bar{I} = \bar{i}$, which leads to an approximate expression for the second threshold:

$${}^2\Lambda_{th} = \frac{\Lambda'_{th}}{1 - \partial \bar{i} / \partial \Lambda \Big|_0 / \partial \bar{I} / \partial \Lambda \Big|_{\Lambda'_{th}}} . \quad (24)$$

A closed form expression is finally obtained:

$${}^2\Lambda_{th} = \frac{(1-\beta)(1+\gamma)}{2(\gamma-\beta)} \Lambda'_{th} . \quad (25)$$

The stability analysis around the steady state yields the following characteristic equation [9]:

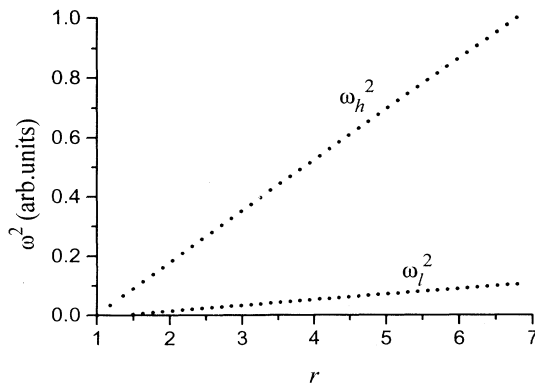


FIG. 5. Evolution of the square of the eigenfrequencies for the bimode state.

$$(\lambda - {}^b\lambda_1)(\lambda - {}^b\lambda_2)(\lambda - {}^b\lambda_3)(\lambda - {}^b\lambda_3^*) \times (\lambda - {}^b\lambda_4)(\lambda - {}^b\lambda_4^*) = 0 , \quad (26)$$

where ${}^b\lambda_1, {}^b\lambda_2$ are real negative numbers for any pumping rate and

$${}^b\lambda_3 = \alpha_l + i\omega_l , \quad (27)$$

$${}^b\lambda_4 = \alpha_h + i\omega_h .$$

The damping coefficient α_l is negative for any pumping rate while α_h is positive in some range of pumping rates for intermediate or high ion-pair concentrations. ω_l and ω_h are, respectively, the low and high frequency of the system. The first one is characteristic of a bimode system (cross saturation) and the second one is associated with the classical relaxation oscillations. The low frequency can be observed in the transient regime provided the two modes are resolved while the higher frequency is always visible in transient regimes (even for the total intensity). The frequencies evolve according to the following rules:

$$\omega_l \propto \sqrt{\Lambda - {}^2\Lambda_{th}} , \quad (28)$$

$$\omega_h \propto \sqrt{\Lambda - {}^1\Lambda_{th}} .$$

This is demonstrated in Fig. 5, which gives the theoretical evolution of ω^2 versus r .

D. Discussion

In this section, we first use the approximate expressions derived previously to fit the experimental values of β and γ which will be used in the numerical analysis.

The cross-saturation parameter (β) can be experimen-

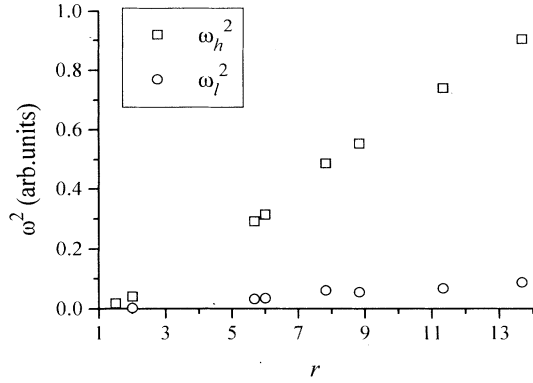


FIG. 6. Experimental evolution of the two eigenfrequencies of an erbium-doped fiber laser with $x = 7.5\%$ (from [3]).

tally determined with the evolution of the two eigenfrequencies of the laser versus the pumping ratio (see Fig. 6). For a two-mode laser these frequencies are related one to the other through the relation [2]

$$\frac{\omega_l^2}{\omega_h^2} = \left[\frac{1-\beta}{1+\beta} \right]^2. \quad (29)$$

The squares of the frequencies are linear functions versus the pump parameter. With the experimental data given in Fig. 6, we obtain $\beta \approx 0.5$.

The anisotropic pumping parameter (γ) can be experimentally obtained using relation (25). Indeed, as previously mentioned, the first lasing threshold is very close to the threshold for the total intensity: ${}^1\Lambda_{th} \cong \Lambda'_{th}$. Under these conditions, (25) leads to

$$\frac{{}^2\Lambda_{th}}{{}^1\Lambda_{th}} \cong \frac{(1-\beta)(1+\gamma)}{2(\gamma-\beta)}. \quad (30)$$

The knowledge of the cross-saturation parameter allows us to estimate γ . Typically, depending on the experimen-

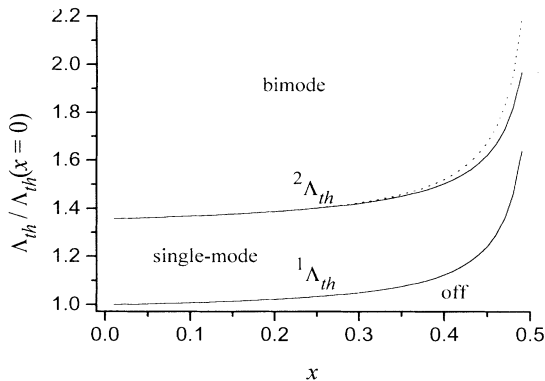


FIG. 7. Exact (solid line) and approximate (dashed line) evolution of the thresholds.

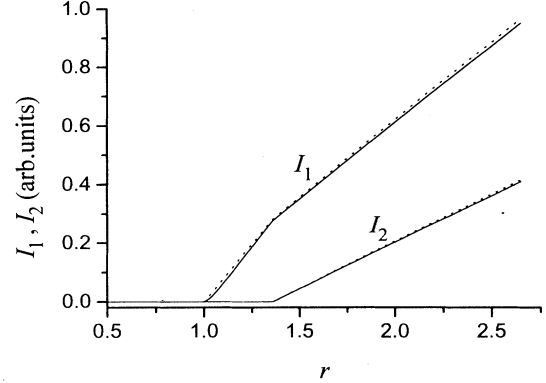


FIG. 8. Exact (solid lines) and approximate (dashed lines) evolution of the steady-state intensities.

tal conditions, the ratio of the thresholds ranges from unity to 2 [3,14], leading to $\gamma = 0.7-1$. In the numerical analysis, we shall take $\gamma = 0.85$. The other parameters used in this paper are [1] $\tau_2 = 10$ ms, $\tau_{22} = 2$ μ s, $\tau_1 = 200$ ns, $N_0 = 5 \times 10^{18}$ cm^{-3} , $\sigma_1 = 1.6 \times 10^{-10}$ $\text{cm}^3 \text{s}^{-1}$, and $y = 0.2$.

Figure 7 gives the evolution of the thresholds versus the ion-pair concentration. The solid lines correspond to the exact solutions (obtained numerically), while the dashed line corresponds to the approximate expression for the second threshold [Eq. (25)]. The thresholds are normalized with ${}^1\Lambda_{th}(x=0)$. These results demonstrate that for $x \leq 0.25$ there is a very good agreement between the exact and approximate thresholds. Typically, the available doped fibers present ion-pair concentrations $x \leq 25\%$ [12]. Note that in the case of perfect symmetry between the two modes, i.e., $\gamma = 1$, both thresholds are equal: ${}^2\Lambda_{th} = {}^1\Lambda_{th} = \Lambda'_{th}$.

Let us now compare the exact and approximate solutions for the intensities. Figure 8 shows the evolution of I_1 and I_2 versus r . The solid lines are the exact solutions obtained by numerical resolution of a third order polynomial, and the dashed lines are the approximate solutions [Eqs. (12), (21), and (23)]. A small discrepancy appears, due to the slight nonlinearity of the exact characteristics: obviously, this discrepancy increases when r increases. Although the approximate solutions do not fit the exact solutions very well, they permit a very good estimation of the second threshold value. The experimental aspect of this point has been reported in [14].

V. NUMERICAL RESULTS

In this section system (8) is numerically solved using a fifth order Runge-Kutta method with an adaptive integration step. We consider different cases of interest: weakly doped fibers (low x) operating in a cw regime and heavily doped fibers (intermediate or high x) operating in a self-pulsing regime. In the second case, the influence of the ion-pair concentration on the dynamics is studied; in particular, the route to chaos (when it occurs) is investigated.

A. Weakly doped fibers: stable steady states

For low x values ($x \leq 5\%$), a cw regime occurs whatever the pumping ratio (stable steady-state solution). In fact, for the particular value $x = 0$, system (8) reduces to

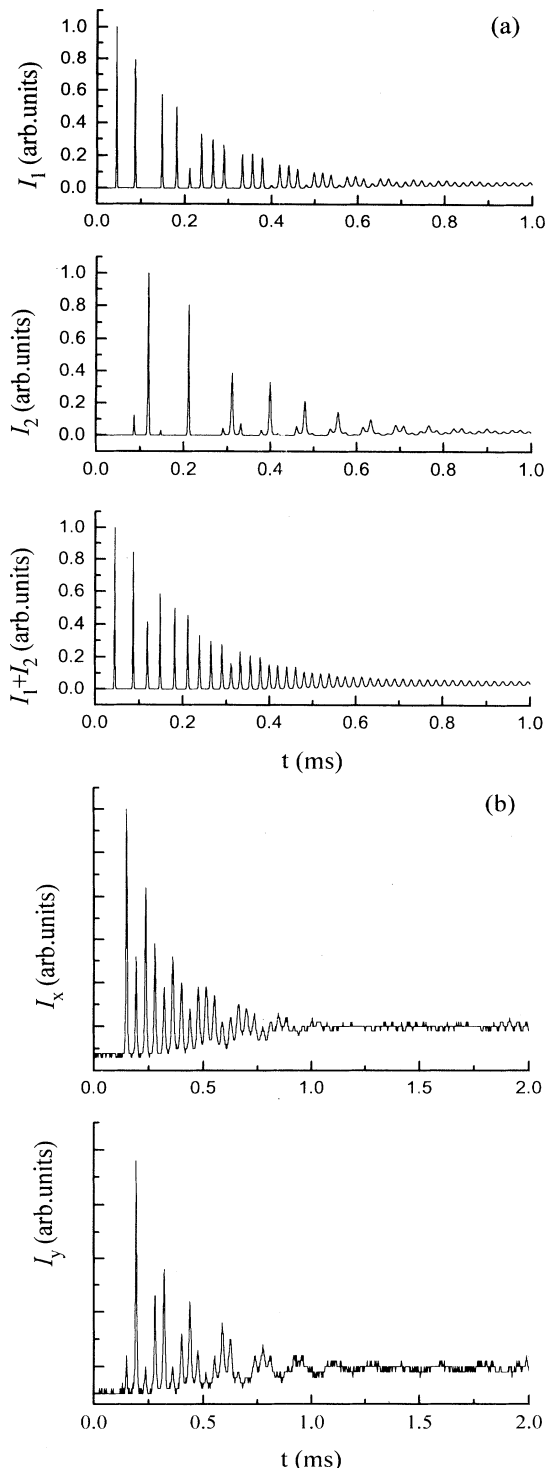


FIG. 9. Transient regime towards the cw operation. (a) Numerical results and (b) experimental data in polarization resolved experiment (from [23]).

the model investigated in [2] which, in turn, corresponds to a classical two-mode laser model [22]. In that case, it is instructive to investigate the transient regime towards the cw operation. This is done in Fig. 9(a) for the two modes and their sum in the case $x = 5\%$. This representation allows the visualization of the eigenfrequencies of the system: the oscillations at the high frequency ω_h (period of about $30 \mu\text{s}$) are in phase between the two modes and the oscillations at the low frequency ω_l (period of about $100 \mu\text{s}$) are in antiphase between the two modes. Similar results are typically obtained in weakly doped fibers. These results confirm the predictions of the linear stability analysis.

The values of the periods obtained numerically are typically two times lower than those measured in wavelength resolved experiments [3,14]. However, the temporal behavior is the same in both cases: the two eigenfrequencies have been observed in either wavelength or polarization resolved experiments. An example of a transient regime in a polarization resolved experiment is given in Fig. 9(b) [23]. The two modes correspond here to the two polarization eigenstates of a weakly doped fiber ($x \approx 5\%$).

B. Heavily doped fibers: from simple to complex dynamics

We call heavily doped fibers those for which the ion-pair concentration is greater than about 6% (unstable steady state). Under such conditions, a great variety of

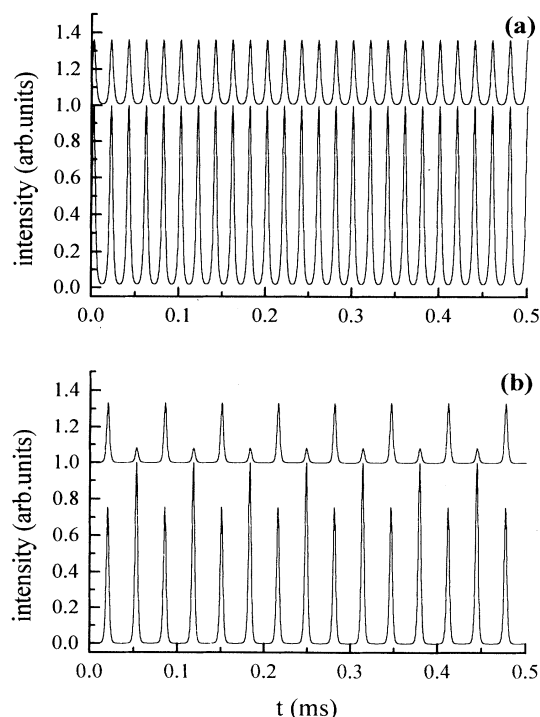


FIG. 10. Time evolution of the two modes for $x = 8\%$: (a) T periodic for $r = 2.25$ and (b) $2T$ periodic for $r = 1.7$. The lower (respectively, upper) curve represents I_1 (respectively, I_2).

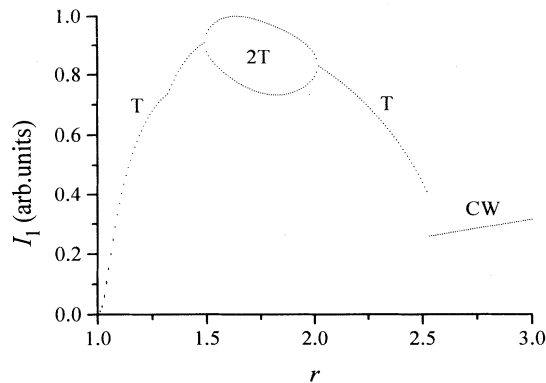


FIG. 11. Bifurcation diagram for $x = 8\%$.

dynamical behavior can be observed depending on the values of x and r . In the following, we investigate some different typical cases for increasing ion-pair concentrations (i.e., $x = 0.08, 0.082, 0.010, \dots$), leading smoothly from simple to more complex dynamics, the pumping ratio being the external control parameter in each case.

1. Case $x = 8\%$

Figure 10 shows two examples of the temporal behavior of the two modes for two pumping rates. A T -periodic self-pulsing regime occurs from $r = 2.25$ and a $2T$ -periodic regime is obtained for $r = 1.7$. These periodic orbits are stable. Note in the case of Fig. 10(b) the antiphase phenomenon which occurs between the two modes [3,14]. In terms of eigenfrequencies, this period doubling can be interpreted as a frequency locking of the low frequency on the subharmonic two of the high frequency. It is more convenient to represent the dynamical scenario on a bifurcation diagram which gives the maxima of the intensity as a function of the pumping rate. This is given in Fig. 11 for the first mode (I_1) in the case $x = 8\%$. For decreasing pumping rates, the system follows the evolution $cw \rightarrow T$ periodic $\rightarrow 2T$ periodic $\rightarrow T$ periodic. The slope breaking appearing near $r = 1.35$ is due to the extinction of the second mode (the weak mode). The transition from a stable cw state to a self-pulsing operation occurs through a Hopf bifurcation [21].

2. Case $x = 8.2\%$

For $x = 8.2\%$, chaotic behavior appears. This is illustrated in Fig. 12, which gives the time evolution of the two modes for different pumping rates: a T -periodic regime is obtained for $r = 2.25$ [Fig. 12(a)], for $r = 2.0$ the system is $2T$ periodic [Fig. 12(b)], $4T$ orbit occurs for $r = 1.81$ [Fig. 12(c)], and finally a chaotic behavior is observed for $r = 1.75$ [Fig. 12(d)]. The corresponding bifurcation diagram is shown in Fig. 13. In this case, the dynamical scenario is $cw \rightarrow T \rightarrow 2T \rightarrow 4T \rightarrow 8T \rightarrow$ chaos (with $4T$ -periodic window) $\rightarrow 4T \rightarrow 2T \rightarrow T$. The chaos is therefore reached through subharmonic bifurcations. In

the chaotic regime, the first return map (not shown here) shows a two-dimensional distribution [9,24], suggesting that the correlation dimension of the strange attractor [25] is between 2 and 3.

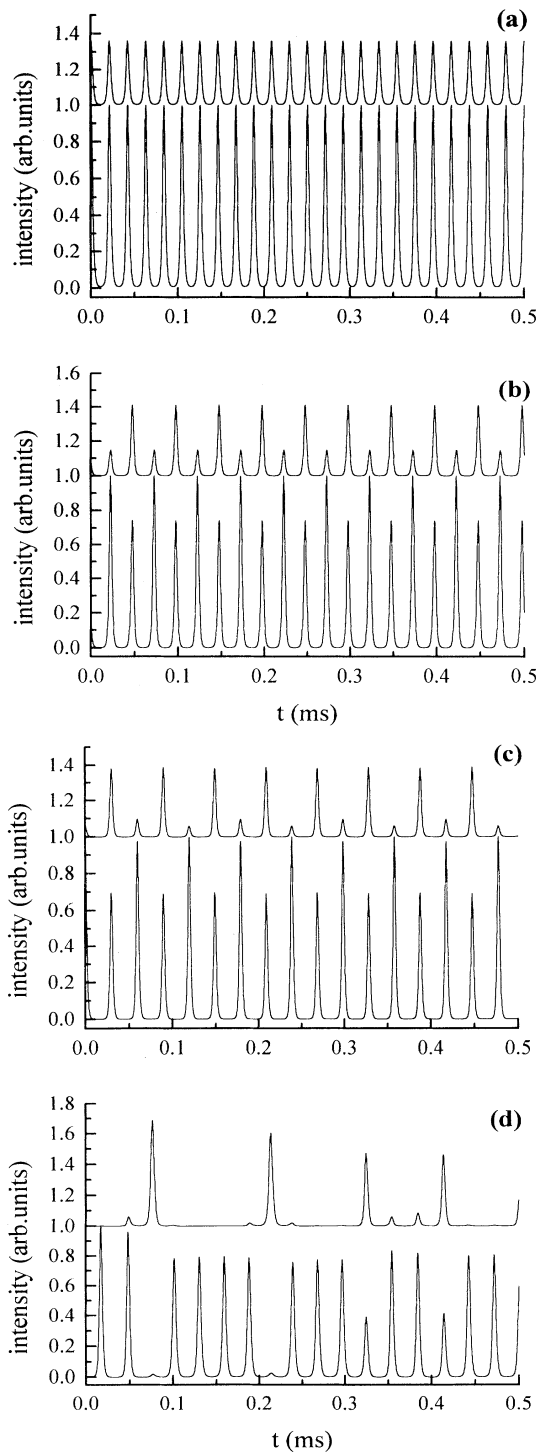
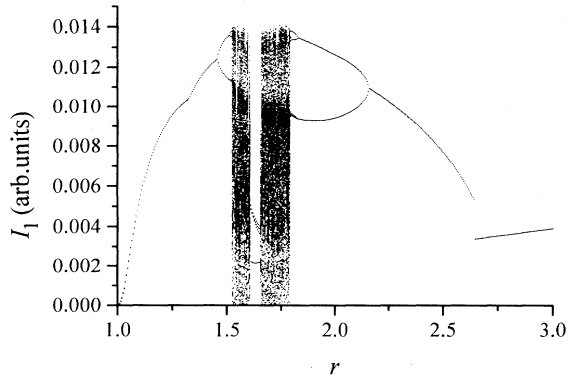


FIG. 12. Time evolution of the two modes for $x = 8.2\%$: (a) T periodic $r = 2.25$, (b) $2T$ periodic $r = 2.0$, (c) $4T$ periodic $r = 1.81$, and (d) chaotic $r = 1.75$. The lower (respectively, upper) curve represents I_1 (respectively, I_2).

FIG. 13. Bifurcation diagram for $x = 8.2\%$.

3. Case $x = 8.5\%$ to $x = 11.5\%$

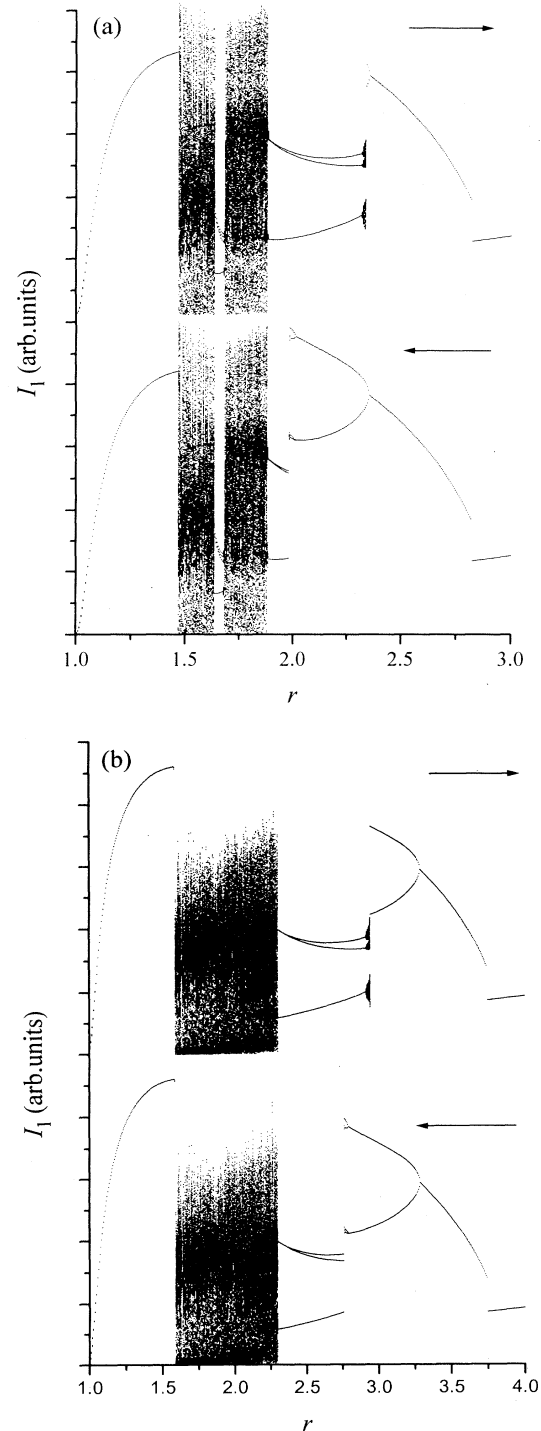
Similar results occur for x ranging from 8.5% to 11.5%. The bifurcation diagrams corresponding to the particular case $x = 8.5\%$ and 10% are given in Fig. 14 for increasing and decreasing pumping rates. The dynamical scenarios are $cw \rightarrow T \rightarrow 2T \rightarrow 4T \rightarrow 8T \rightarrow 3T \rightarrow \text{chaos} \rightarrow T$, for decreasing r and $T \rightarrow \text{chaos} \rightarrow 3T \rightarrow \text{QP}$ (quasiperiodic motion) $\rightarrow 2T \rightarrow T \rightarrow cw$, for increasing r values. As shown in the diagrams, a generalized bistability occurs between the $2T$ - and the $3T$ -periodic orbits. The range of pumping ratio for which this bistability is observed decreases while x increases. The calculated correlation dimension of the chaotic attractor around $r = 1.75$ is about 2.8 in the case $x = 10\%$ [9]. The QP regime is easily pointed out with the help of a first-return map which exhibits a closed one-dimensional curve (with several possible branches); the attractor is a torus T^2 in the phase space [26]. An example is shown in Fig. 15 for the ion-pair concentration $x = 10\%$ and $r = 2.8$.

From the experimental point of view, we have observed the evolution $cw \rightarrow T \rightarrow 2T \rightarrow 3T \rightarrow \text{chaos} \rightarrow T$ for decreasing r values in the case $x = 7.5\%$ [3] (the same behavior was observed for increasing r). The QP regime has also been observed experimentally in [3] between the $2T$ and $3T$ regimes in a narrow range of pumping rates. Nevertheless, no attention was given in this work to any bistability. The predicted $4T$ - and $8T$ -periodic regimes seem difficult to observe because they are localized in very small pumping rate ranges. Note that the results presented here for $x = 10\%$ complement those in Ref. [9]: the periodic orbits $4T$ and $8T$ have not been previously reported, nor has the bistability been obtained versus r .

4. Case $x \geq 12\%$

In this paragraph we investigate the case where $x = 12\%$ and the results obtained are similar for higher

ion-pair concentrations. No bistability is obtained for this range of x . The bifurcation diagram is presented in Fig. 16. The dynamical scenario for decreasing r values is $cw \rightarrow T \rightarrow 2T \rightarrow 4T \rightarrow 8T \rightarrow \text{QP} \rightarrow \text{chaos} \rightarrow \text{QP}$

FIG. 14. Bifurcation diagram for (a) $x = 8.5\%$ and (b) $x = 10\%$ for increasing and decreasing pumping rates.

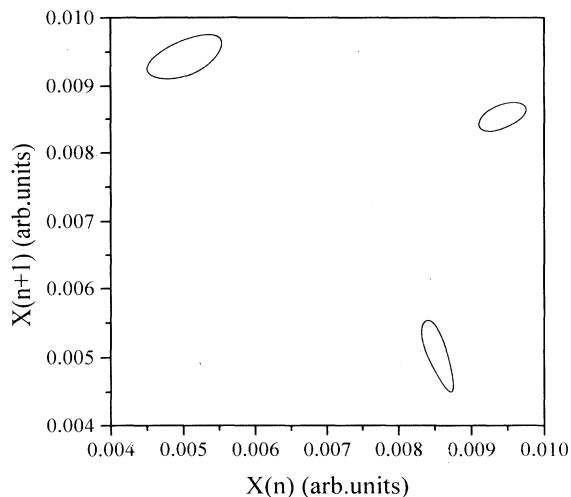


FIG. 15. First-return map for $x = 10\%$ and $r = 2.8$.

$\rightarrow 3T \rightarrow$ chaos (with periodic windows) $\rightarrow T$. Figure 17 gives more information about the transition between the $8T$ -periodic orbit and the chaotic regime. Figure 17(a) represents a phase portrait of the attractor in the plane (I_1, I_2) for $r = 3.8425$; the corresponding first-return map is shown in Fig. 17(b). A QP regime is clearly obtained; the calculated correlation dimension is very close to 2. This QP regime is localized in a very narrow range of pumping rates as demonstrated in Fig. 18, which gives first-return maps for lower r values. Figure 18(a) shows the progressive destruction of the torus for $r = 3.8410$ towards a strange attractor for $r = 3.82$ [Fig. 18(b)]. At the same time, the dimension of the attractor evolves from 2 (torus) to a fractal dimension of 2.3 (strange attractor). By decreasing r , the system falls again in quasiperiodic motion, as shown in Figs. 18(c) and 18(d), which progressively evolves towards a stable $3T$ -periodic orbit. This periodic orbit can be interpreted again as a frequency

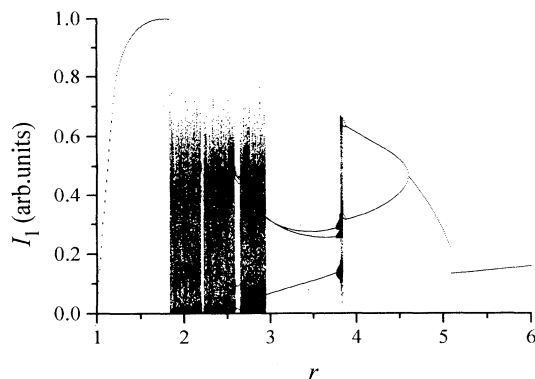


FIG. 16. Bifurcation diagram for $x = 12\%$.

locking of the low frequency but this time on the subharmonic 3 of the high frequency of the system [26]. A chaotic behavior with some periodic windows is finally reached. Its correlation dimension is higher than the previous one.

Previous results (for ion-pair concentrations allowing a chaotic dynamics) show unusual routes to chaos. In fact, the known routes to chaos are based on bifurcations with codimension 1 [26]. Our results demonstrate that the codimension is 2. The control parameter space needed to observe the whole dynamics is two dimensional (x, r) .

VI. CONCLUSIONS

This paper has been devoted to a detailed study of analytical and numerical results obtainable from our previous model describing erbium-doped fiber lasers dynamics. A summary of the single-mode model has been included. In addition, an approximate solution (at first order with respect to the pumping parameter) for the inten-

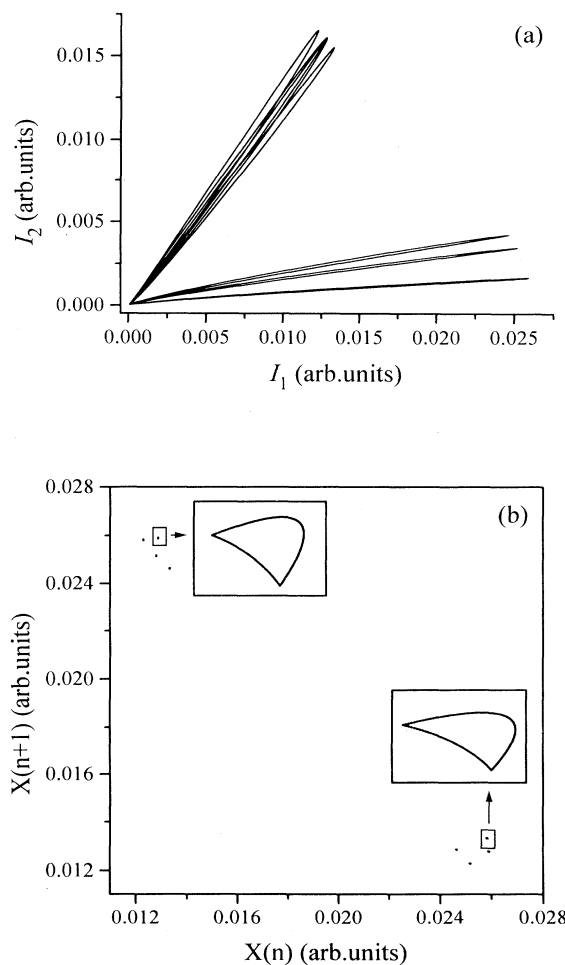


FIG. 17. (a) phase diagram in QP regime for $r = 3.8425$ and (b) first-return map in QP regime.

sity is derived using the fact that the gain saturates to its value at threshold. Numerical simulations show that a self-pulsing regime occurs for heavily doped fibers. This instability is due to the quenching effect between two excited neighboring ions resulting in a fast saturable absorption.

A two-mode model has been presented and investigated with respect to the ion-pair concentration and the pumping ratio. The stationary states (off state, single-mode state, and bimode state) are derived and a linear stability analysis has been performed. In the same way as for the single-mode model, approximate solutions for the intensities have been analytically obtained, leading to a very good approximate expression for the second laser threshold (associated to the weak mode). These results lead to a simple experimental determination of both the

anisotropic pumping and the cross-saturation parameters.

The numerical simulations had revealed a great variety of dynamical behaviors. For weakly doped fibers ($x \leq 5\%$), stable steady states are obtained and the results are similar to those of a classical two-mode laser model. A self-pulsing instability (T periodic and $2T$ periodic) occurs in some range of pumping rates for x ranging from about 6% to 8%. In the particular case where $x = 8\%$, the dynamical scenario for decreasing r is $\text{cw} \rightarrow T$ periodic $\rightarrow 2T$ periodic $\rightarrow T$ periodic. The $2T$ orbits can be viewed as a frequency locking of the low frequency on the subharmonic 2 of the high frequency.

For slightly higher pair concentrations, a chaotic dynamics appears. For $x = 8.2\%$, the chaos is reached through successive subharmonics bifurcations. In the

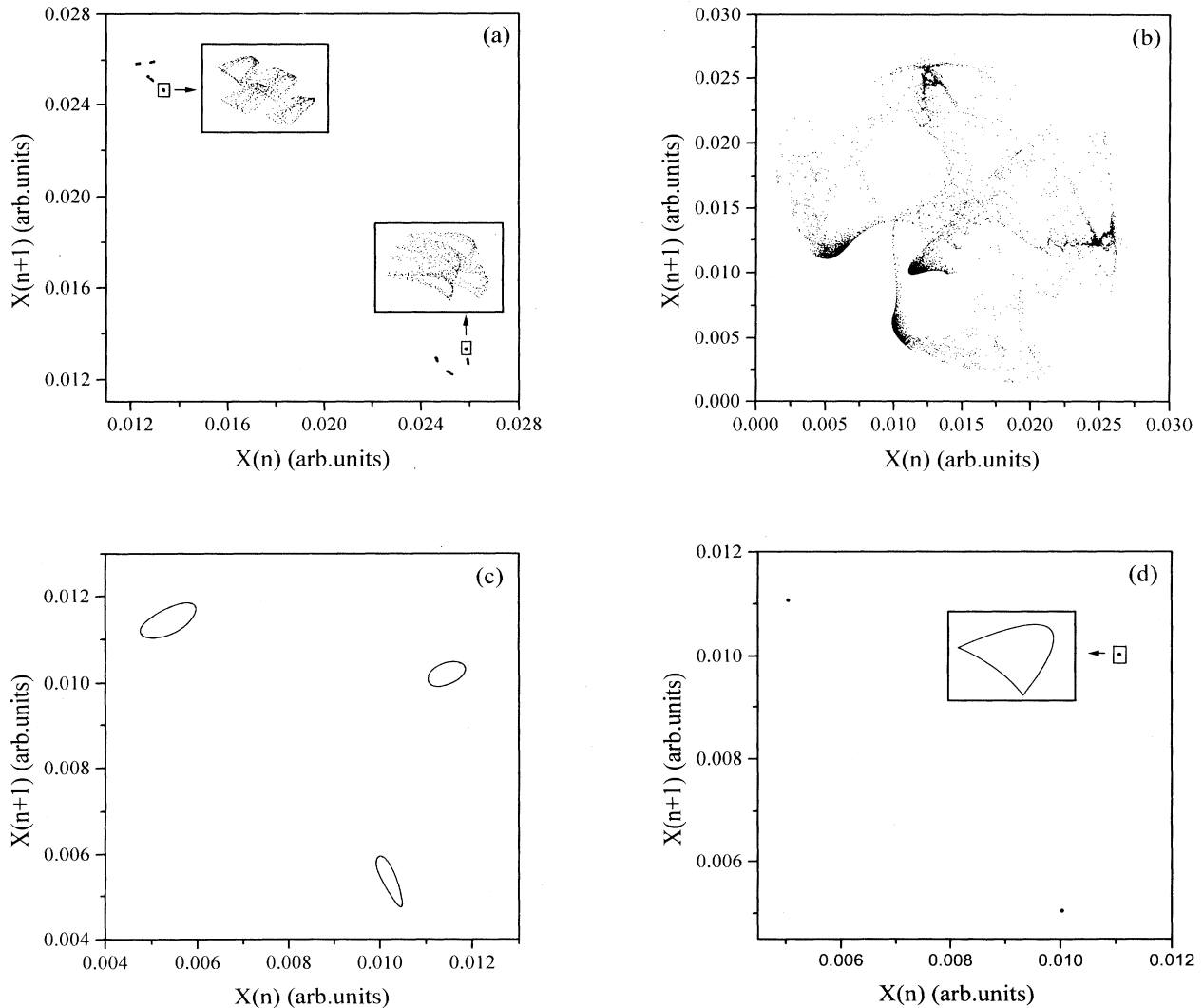


FIG. 18. First-return map: (a) $r = 3.8140$, (b) $r = 3.82$, (c) $r = 3.78$, and (d) $r = 3.7$.

case where x ranges from about 8.5% to 11.5%, a bistability between $2T$ - and $3T$ -periodic orbits occurs versus r . This implies the coexistence of two stable periodic attractors. For example, when the system is in a $3T$ orbit and r is increased, the system evolves towards a stable T^2 torus which, when it becomes unstable, leads to a sudden switch towards the stable $2T$ orbit. In the opposite case, where r is decreased, a sudden switch occurs between the $8T$ orbit (which leads to chaos) and the stable $3T$ -periodic orbit. Lastly, the case $x = 12\%$ has been studied with particular attention. In that case, the system does not exhibit bistability versus r . The scenario for decreasing pumping rates is $cw \rightarrow T \rightarrow 2T \rightarrow 4T \rightarrow 8T \rightarrow QP \rightarrow \text{chaos} \rightarrow QP \rightarrow 3T \rightarrow \text{chaos}$ (with periodic windows) $\rightarrow T$. The first QP regime is localized in a very narrow range of r values. We have observed the progressive destruction of the torus towards a strange attractor and finally the reconstruction of a new torus. Numerical re-

sults also demonstrated an unusual route to chaos.

Some of the theoretical results presented here have been experimentally observed [1,3,11–14]. Nevertheless, some points remain which need supplementary experimental work: the bistability between periodic orbits and the different route to chaos. The practical problem here is essentially to obtain the adequate fiber with particular ion-pair concentration; this last parameter is difficult to control during the elaboration process of the fiber. An attractive method to overcome this problem will be the use of two sliced erbium fibers, respectively weakly and heavily doped. The resulting ion-pair concentration can be monitored by adjusting the respective lengths of the fibers. From the theoretical point of view, it will be interesting to investigate in the phase space (three dimensional) the evolution of the attractors, in particular, the transformation of a periodic or quasiperiodic attractor into a strange attractor.

-
- [1] F. Sanchez, P. Le Boudec, P. L. François, and G. Stephan, *Phys. Rev. A* **48**, 2220 (1993).
- [2] S. Bielawski, D. Derozier, and P. Glorieux, *Phys. Rev. A* **46**, 2811 (1992).
- [3] F. Sanchez, M. Le Flohic, G. M. Stephan, P. Le Boudec, and P. L. François, *IEEE J. Quantum Electron.* **QE-31**, 881 (1995).
- [4] D. Pureur, M. Douay, P. Bernage, P. Niay, E. Delevaque, S. Boj, J.-F. Bayon, and H. Poignant, *J. Phys. (France) III* **5**, 237 (1995).
- [5] K. Wiesenfeld, C. Bracikowski, G. James, and R. Roy, *Phys. Rev. Lett.* **65**, 1749 (1990).
- [6] M. Georgiou, and P. Mandel, *IEEE J. Quantum Electron.* **QE-30**, 854 (1994).
- [7] K. Otsuka, *Phys. Rev. Lett.* **67**, 1090 (1991).
- [8] R. Leners and G. Stephan, *Quantum Semiclass. Opt.* **7**, 757 (1995).
- [9] F. Sanchez, M. Le Flohic, P. Besnard, P. L. François, and G. M. Stephan, *J. Phys. (France) III* **5**, 281 (1995).
- [10] S. Bielawski and D. Derozier, *J. Phys. (France) III* **5**, 251 (1995).
- [11] P. Le Boudec, M. Le Flohic, P. L. François, F. Sanchez, and G. Stephan, *Opt. Quantum Electron.* **25**, 359 (1993).
- [12] P. Le Boudec, P. L. François, E. Delevaque, J.-F. Bayon, F. Sanchez, and G. Stephan, *Opt. Quantum Electron.* **25**, 501 (1993).
- [13] E. Lacot, F. Stoeckel, and M. Chenevier, *Phys. Rev. A* **49**, 3997 (1994).
- [14] P. Le Boudec, F. Sanchez, C. Jaouen, P. L. François, J.-F. Bayon, P. Besnard, and G. Stephan, *Opt. Lett.* **18**, 1890 (1993).
- [15] P. F. Wysocki, J. L. Wagener, M. J. F. Dignonnet, and H. J. Shaw, *Proc. SPIE* **1789**, 66 (1992).
- [16] F. Auzel, D. Meichemin, F. Pellé, and P. Goldner, *Opt. Mater.* **4**, 35 (1994).
- [17] J. L. Wagener, P. F. Wysocki, M. J. F. Dignonnet, H. J. Shaw, and D. J. Di Giovanni, *Opt. Lett.* **18**, 2014 (1993).
- [18] J. L. Wagener, P. F. Wysocki, M. J. F. Dignonnet, and H. J. Shaw, *Opt. Lett.* **19**, 347 (1994).
- [19] E. Delevaque, T. Georges, M. Monerie, P. Lamouler, and J.-F. Bayon, *IEEE Phot. Tech. Lett.* **5**, 73 (1993).
- [20] A. Kellou, H. Ladjouze, F. Sanchez, and G. M. Stephan, *Opt. Quantum Electron.* **27**, 741 (1995).
- [21] G. Iooss and D. D. Joseph, *Elementary Stability and Bifurcation Theory*, Undergraduate Texts in Mathematics (Springer-Verlag, New York, 1990).
- [22] H. Statz and G. DeMars, *J. Appl. Phys.* **35**, 1377 (1964).
- [23] B. Meziane, F. Sanchez, M. LeFlohic, P. L. François, and G. Stephan (unpublished).
- [24] K. Tanii, M. Tachikawa, T. Tohei, F.-L. Hong, and T. Shimuzu, *Phys. Rev. A* **43**, 1498 (1991).
- [25] P. Grassberger, and I. Procaccia, *Phys. Rev. Lett.* **50**, 346 (1983).
- [26] P. Bergé, Y. Pomeau, and C. Vidal, *Order Within Chaos* (Wiley, New York, 1984).